Broadband Tunable Electron Paramagnetic Resonance Spectroscopy of Dilute Metal Complexes

Hagen, Wilfred R.

DOI
10.1021/acs.jpca.9b03574

Publication date
2019

Document Version
Final published version

Published in
Journal of Physical Chemistry A

THE JOURNAL OF PHYSICAL CHEMISTRY A

Article

Cite This: J. Phys. Chem. A 2019, 123, 6986−6995

pubs.acs.org/JPCA

Broadband Tunable Electron Paramagnetic Resonance Spectroscopy of Dilute Metal Complexes

Wilfred R. Hagen*

Department of Biotechnology, Delft University of Technology, Van der Maasweg 9, 2629HZ Delft, The Netherlands

Supporting Information

ABSTRACT: Analysis of the electron paramagnetic resonance (EPR) of transition ion complexes requires data taken at different microwave frequencies because the spin Hamiltonian contains operators linear in the frequency as well as operators independent of the frequency. In practice, data collection is hampered by the fact that conventional EPR spectrometers have always been designed to operate at a single frequency. Here, a broadband instrument is described and tested that operates from 0.5 to 12 GHz and whose sensitivity approaches that of single-frequency spectrometers. Multifrequency EPR from triclinic substitutional (0.5%) Cu(II) in $ZnSO_4$ is globally analyzed to illustrate a novel approach to reliable determination of the molecular electronic structure of transition ion complexes from field-frequency 2D data sets.

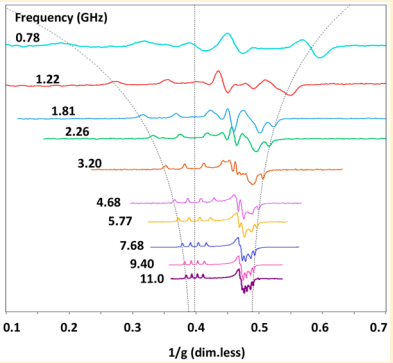

INTRODUCTION

The technique of electron paramagnetic resonance (EPR) is of considerable value for the determination of structural and electronic properties of transition-metal complexes. Ever since 1947[1] until this day the vast majority of studies have been done with microwaves at a single frequency in the X-band around 9.5 GHz. Since the spectra of these compounds are often determined by a combination of frequency-dependent and frequency-independent interactions, their deconvolution benefits from taking data at microwave frequencies outside X-band. Typical problems whose solution requires multifrequency data are, e.g., analysis of poorly resolved metal hyperfine interaction, disentanglement of overlapping hyperfine spectra from multiple centers, identification of low-symmetry (monoclinic, triclinic) coordination, and determination of spatial and redox relations through dipolar-interaction measurement in multicenter metalloproteins. In practice, this raises an issue of availability of spectrometers operating at other than X-band frequencies: conventional EPR spectrometers have long been[2] single-frequency devices in which a narrowband source of microwaves is combined with a cavity resonator as sample holder. The high resonator quality factor of the cavity ensures practical concentration sensitivity for chemical and biochemical applications, but its single-frequency operation implies that multifrequency spectroscopy requires the use of several spectrometers.

I have earlier worked out the concept of replacing the resonator with a coaxial transmission line in which the paramagnetic sample acts as part of the dielectric that separates the inner and outer conductor.[3] Unfortunately, in this transmission EPR spectroscopy the advantage of broad frequency tunability is counteracted by very low sensitivity of the transverse electromagnetic (TEM) transmission line. It was, however, found that, in the very low gigahertz range, the loss of sensitivity could be partially compensated by increasing the length of the transmission line up to a limit determined by per-length dielectric losses. The maximum length of the line was furthermore limited by geometrical constraints of the magnet, and miniaturization of the line's axial dimensions was proposed as a future development to lead to reduction in sample size, to increase in the TEM frequency cutoff, and to yield more practical cell dimensions for cryogenic experimentation.

Since reduction of paramagnet-filled coaxial line dimensions poses a considerable engineering challenge, I have searched for possible alternative implementations of transmission EPR that would be more suitable for miniaturization. Here I describe development of such quasi-TEM cells using wire micro strip as the transmission medium in which the paramagnetic sample is one of the dielectric phases. It turns out that these cells, when combined with transmission lines of significant lengths in combination with a tunable phase shifter to adjust the optical-path length, actually form multimode resonators with high *Q*-factors. These broadband-tunable circuits form the basis for the construction of a *single* sensitive EPR spectrometer for the detection of transition-metal complex spectra at an essentially unlimited number of frequencies and illustrated here for the approximate range of 0.5−12 GHz (i.e., UHF-, L-, S-, C-, and X-band). Below, I describe the theory, engineering, and testing of a sensitive broadband spectrometer, and I illustrate its applicability in a multifrequency study of a dilute Cu(II) model coordination compound in a crystal of triclinic symmetry.

Received: April 16, 2019
Revised: July 1, 2019
Published: July 18, 2019

DOI: 10.1021/acs.jpca.9b03574
J. Phys. Chem. A 2019, 123, 6986−6995

RESULTS

Spectrometer Design: The Sample Cell. At the heart of the broadband spectrometer is a sensitive transmission/reflection device that must be tunable to a large number of closely spaced resonance frequencies over a wide frequency span. A key component in the construction of this cell is the use, as microwave transmission medium, of a long stretch of "wire micro strip" folded into a small geometric structure. The wire micro strip principle is illustrated in Figure 1A: on top of a conducting base plate, covered with a dielectric insulator, is a conducting wire of circular cross section surrounded by air ($b = 0$) or by an additional layer of the dielectric medium ($b \neq 0$). When current flows through the wire and returns through the ground plate, electric field lines are set up between the wire and the plate. Magnetic field lines develop perpendicular to the **E** lines, and they form the alternating magnetic field that induces microwave transitions. This time-dependent field, that is, the microwave magnetic field incident on the sample, is usually denoted as $\mathbf{B}_1$ to discriminate it from the static field $\mathbf{B}_0$ of the slowly scanning electromagnet that creates the magnetic ground manifold of energy states of the compound under study. The field lines of $\mathbf{B}_1$ are perfectly parallel to the base in between the wire and the base, but they diverge on both sides of the wire (Figure 1A). However, when we orient the wire's long axis along the $\mathbf{B}_0$ vector, then the $\mathbf{B}_1$ lines are always perpendicular to $\mathbf{B}_0$ as they should be for regular EPR spectroscopy.

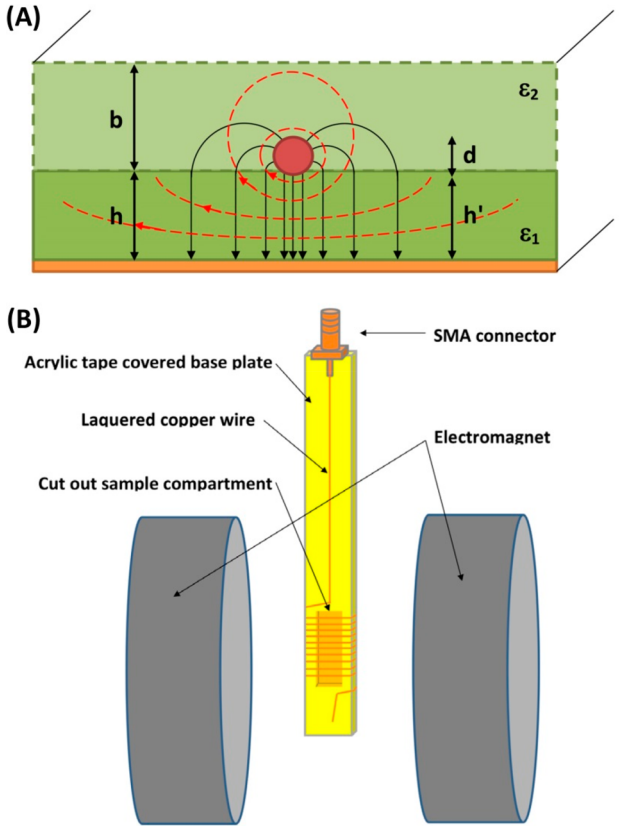

Figure 1. Wire micro strip as a basis for multimode broadband EPR resonators. (A) Schematic illustration (cross section) of wire micro strip: a copper wire of diameter d passes over a copper base plate at a height of h' mm with a diamagnet ε_1 (green) as insulator. The wire can be surrounded by air ($b = 0$) or by a second insulator ε_2 (light green) of height b. Solid black lines are electric-field lines; broken red lines are magnetic-field lines. (B) EPR reflection cell based on wire micro strip in which some of the diamagnetic isolator is replaced with paramagnetic sample (orange rectangle). A long optical path is created by having the wire repeatedly pass over the sample in parallel turns. The shown geometry ensures that the microwave $\mathbf{B}_1$ field in the EPR sample is everywhere perpendicular to the external static field **B**.

The cell is now constructed as follows (Figure 1B). A rectangular base plate of pure copper metal, with a thickness (i.e., smallest dimension) of 1 mm to obtain a sturdy structure, is covered with layers of acrylic tape as the diamagnetic medium. A rectangular volume is cut away from the acrylic tape on one side, or on both sides, of the cell to create a space to hold the EPR sample. In other words, the removed part of the diamagnetic is to be replaced by paramagnetic material. Then a lacquered copper wire of 0.2 mm diameter is regularly wound around the cell, keeping sufficient space between windings (≥1.0 mm) to avoid electronic cross talk. The ends of the wire are made bare and are soldered to the inner conductor of coaxial connectors of the SMA type, whose ground is soldered to the short ends of the rectangular base plate. We have thus constructed a cell operating in transmission mode. Leaving out one of the SMA connectors, and leaving one end of the wire either open or soldered to the base plate, creates a cell operating in reflection mode. The latter is particularly suited for cryogenic applications: it can be hung from a connecting coax cable into a conventional helium flow dewar between the poles of an electromagnet. And when the geometry is chosen as in Figure 1B, then the wire segments over the paramagnetic sample all run parallel to the $\mathbf{B}_0$ axis, and thus all $\mathbf{B}_1$ lines that penetrate the paramagnetic sample are in a plane perpendicular to $\mathbf{B}_0$. A technical (3D isometric) drawing can be found in the Supporting Information, part A, Cell Design.

A proper set of values for the geometric parameters in Figure 1A, i.e., the height of the lower phase h', the diameter of the wire, d, and the height of the upper phase b, can be estimated from the universal impedance value of $Z = 50\ \Omega$ for microwave components in combination with an empirical approximative expression for the impedance of a *square* wire micro strip of width w over a dielectric of height h:[4−7]

$$Z = \frac{Z_{\text{air}}}{2\pi\sqrt{\varepsilon_{\text{eff}}}} \operatorname{arccosh}\left(\frac{2h + w}{w}\right) \tag{1}$$

in which

$$\varepsilon_{\text{eff}} = \left(\frac{\varepsilon_{\text{R}} + 1}{2}\right) + \left(\frac{\varepsilon_{\text{R}} - 1}{2}\right)\sqrt{\frac{w}{w + 12h}} \tag{2}$$

This square-wire expression becomes applicable to round wire, with diameter d, by the substitutions

$$w = 0.8472 \times d \tag{3}$$

$$h = h' + 0.0915 \times w \tag{4}$$

Here $Z_{\text{air}} = 377\ \Omega$ is the characteristic impedance of air, ε_{R} is the relative electric permittivity of the isolator phase, and ε_{eff} is its effective value for the given geometry. An additional correction for a wire embedded in an extended isolator phase ($b \neq 0$) can be found in the Supporting Information, part B, Theory, where the theoretical background for these equations is discussed. If we now take a lacquered copper wire of $d = 0.2$ mm diameter, which is thick enough to avoid regular wire breaking and at the same time small enough to allow for several windings sufficiently separated to avoid cross talk, then for an

DOI: 10.1021/acs.jpca.9b03574
J. Phys. Chem. A 2019, 123, 6986−6995

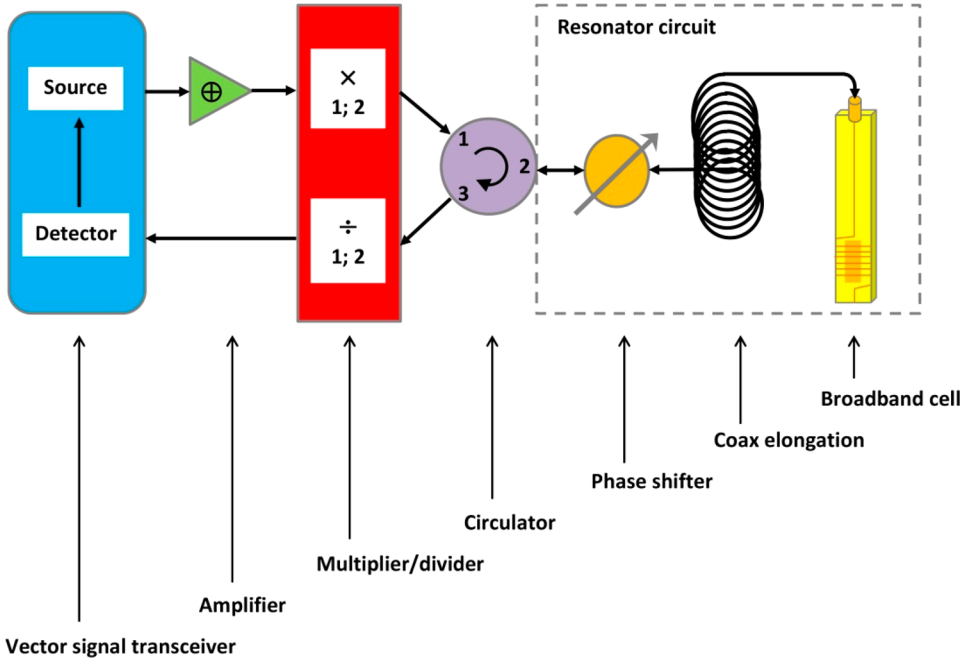

Figure 2. Outline of the microwave part of the broadband reflection spectrometer. Schematic with components as indicated. (See main text and Supporting Information for details.) In the resonator circuit that starts, and ends, at port 2 of the circulator, standing microwaves are set up that become attenuated when the paramagnetic sample in the broadband cell experiences the EPR effect.

isolator thickness of $h' = 0.2$ mm (i.e., four covers of 0.05 mm acrylic tape) and minor embedding ($b = 0.1$), we find a permittivity $\varepsilon_R \approx 5$, which is roughly an intermediate value for inorganic salts, in order to end up with a characteristic impedance of $Z \approx 50\ \Omega$. We have herewith created a low-loss, multimode (see Figure 2, below) resonator. In practice, there will be discontinuity losses, e.g., at the boundaries between sample and acrylic, but also dielectric attenuation, which is linear in the wire length and in the microwave frequency (Supporting Information, part B, Theory). In addition, we want to purposefully create paramagnetic loss by bringing the sample into resonance. This extra loss is measured as the EPR signal; it is linear in the sample's paramagnetism (or imaginary relative magnetic permeability) and also in the length of the wire over the sample and in the microwave frequency as detailed in the Supporting Information.

Spectrometer Design: The Resonator Circuit and Its Operation. Connecting the two ends of the transmission cell with coax cables to a source and a detector of microwaves and placing the cell in the field of an electromagnet create a transmission EPR spectrometer. A mode pattern is set up between the discontinuities created by the cell's SMA connectors; however, the pattern is very shallow (Supporting Information, part C, Mode Patterns) and the resonance peaks have poor loaded quality factors $Q \leq 10$, where Q is defined as the resonance frequency divided by the peak width at a detection power 3 dB above that of the negative-peak power:

$$Q = \frac{\nu_{res}}{\Delta\nu_{3dB}} \tag{5}$$

The reflection version of the cell, with one SMA connection omitted and with the end of the wire of length L disconnected, behaves like the microwave equivalent of an open organ pipe of length L in which well-defined resonances are set up at even integers $2n$ of a quarter wavelength, with wave velocity c_0:

$$\nu_{res} = \left(\frac{2n}{4}\right)\frac{c_0}{L} \tag{6}$$

With the cell connected to a source and detector via a three-port circulator, as in Figure 2, the loaded Q factor now increases by an order of magnitude. Since the only practical way of further increasing this number is to increase the length of the cell (at the expense of some line attenuation) we insert a long (up to a few meters) piece of coax cable between the circulator and the cell, and this results in an order of magnitude increase in the number of tunable resonances and some 2 orders of magnitude increase in their Q factor to values of order 10^4. Finally, we make the path of the resonator (and therefore its resonance frequencies) adjustable by the insertion of a broadband, "trombone" type phase shifter. The whole resonator structure now starts and ends at port 2 of the circulator as outlined in Figure 2. Since high-quality microwave circulators have a limited frequency span, a set of six different circulators is used substitutionally to cover the range 0.5−12 GHz.

A National Instruments vector signal transceiver (VST) is used as a programmable, solid-state source and detector of microwaves in the range from 65 MHz to 6 GHz. Maximum power output of 12 dBm is boosted with a broadband amplifier to some 25 dBm or 250 mW. Between the VST and the circulator, a home-built frequency multiplier structure is placed to extend the frequency range to at least 12 GHz. Details of this multiplier and the other microwave equipment, the electromagnet, and the helium flow system are given in the Supporting Information, part D, Hardware.

A typical EPR experiment proceeds as follows. With the microwave source set to an intermediate output level, e.g., 0 dBm, i.e., 1 mW, a scan is made of the power reflected by the resonator circuit as a function of the frequency over the range available for the used circulator. Inspection identifies a resonance peak, or "dip", near the frequency of interest. In a

DOI: 10.1021/acs.jpca.9b03574
J. Phys. Chem. A 2019, 123, 6986−6995

subsequent, real-time procedure (described in detail in the Supporting Information, part E, Software) this dip is optimized for maximal loaded Q value. Then, complex IQ (in-phase and quadrature) data are collected at high rate, typically some 10^6 signals per second, online converted to real values of reflected power, and online processed to a numerically filtered standard size of 1024 field points. Field scans are made, e.g., in 20 s, and no electronic RC filter is employed. This setup implies a fast data acquisition rate on the order of 10^4 averages per spectral point, which is essential for the attained signal-to-noise ratio of the final spectra. Data from forward and reverse scans are continuously collected and averaged to a final EPR absorption spectrum, which is numerically differentiated for ease of comparison with conventional EPR data. In case the spectrum is partially dispersive, it is turned into a pure absorption by means of a Hilbert transform according to Ernst's procedure.[8] All data acquisition and manipulation software has been written in LabVIEW with some of the more computationally demanding routines inserted as dynamic link libraries written in Intel Visual FORTRAN (see the Supporting Information, part E, Software).

Spectrometer Testing on Dpph Model Spectra. As a test of monochromaticity, stability, and resolution, the single-line spectrum of solid 2,2-diphenyl-1-picrylhydrazyl (dpph) powder has been measured at ambient temperature over a wide field scan as a function of the frequency (Figure 3).

The reflection cell has a base plate of 6.5 mm width and an extended length of 400 mm. The goal of the latter is to have the SMA connector well outside the magnetic field since in a previous work I found SMA connectors to contain an $S = 1$ paramagnet whose very broad EPR signal shows up as a sloping baseline.[3] The sample compartment is 80 × 4 × 0.2 mm, i.e., a volume of 64 μL. With 80 windings, the total wire length (i.e., optical path) from the SMA connector to the open end is some 130 cm. Slow single forward scans were recorded over 180 s over a field range of 0−4500 G. Resonance frequencies (dips) in the range 0.5−12 GHz were chosen to be approximately separated by 0.5 GHz. A 2D stack plot of the results is presented in Figure 3. The separations between baseline levels (vertical axis) and the separations between dpph signals (horizontal axis) are not constant because the dips are not exactly spaced at 0.5 GHz intervals. Note that all zero crossings connect through a straight line diagonal over the figure, attesting to the linearity of the electronic Zeeman interaction in the microwave frequency.

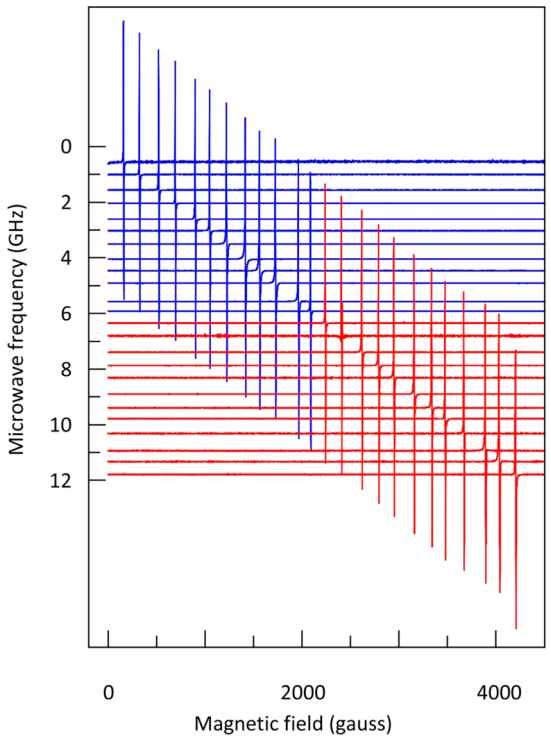

Figure 3. Broadband system test on a sharp line over a wide field range. The single, sharp line (<3 G peak-to-peak) of solid dpph was measured in single, slow (180 s) scans of 4500 G in 6000-point resolution over the approximate frequency range 0.5−12 GHz in frequency steps of ca. 0.5 GHz (i.e., 24 frequencies). The baseline of each spectrum has been *y*-axis positioned to the employed frequency value. Spectral color code: blue, nonmultiplied frequencies; red, frequency-doubled.

Then the response of the spectrometer to changes in microwave power level was studied with the same reflection cell by measuring the dpph spectrum now over a narrow field range of 80 G and at a single frequency of 2.6 GHz. The latter value was chosen to be in the base range of the VST (i.e., <6 GHz) and within the range of an available high-power (output: 43 dBm or 15 W) broadband amplifier (0.8−2.7 GHz). Field-forward and field-reverse scans each of 20 s were collected and combined for increased signal-to-noise ratio. The spectrometer can be operated over at least 13 decades of microwave power (Figure 4A).

The integrated intensity of the EPR spectrum is essentially linear in the applied power. At power levels above the highest value reported here (34 dBm or 1.56 W, ambient temperature, no cooling), the system becomes increasingly unstable by produced heat. A pure absorption spectrum is obtained over a power range of some 60 dB, namely, from circa −50 to +10 dBm. Outside these limits, increasingly a Hilbert rotation correction[8] is required to transform partially dispersive spectra into pure absorptions (Figure 4C,D). Implementation of the correction of experimental spectrum S_{exp} to absorption spectrum $S_{absorption}$ is as follows:

$$S_{absorption} = \frac{\alpha H(S_{exp}) - \mathrm{sig}(1-\alpha)S_{exp}}{\sqrt{\alpha^2 + (1 - \mathrm{sig}(\alpha))^2}} \quad (7)$$

in which α is the rotation factor in the range −1 to +1 (0 for pure absorption and ±1 for pure dispersion), sig is the sign of α, and H is the fast Hilbert transform routine from LabVIEW's Signal Processing Virtual Instruments library. At the higher end of the power spectrum (microwatt to watt) the loaded quality factor Q of the resonator circuit, as measured by fitting a Lorenzian to the dip pattern, is very high, namely, on the order of (1−2) × 10^4. Below an incident power of 1 μW Q decreases linearly and extrapolates to unity at ca. 100 fW (Figure 4E,F). Note that the here determined loaded Q factor is a characteristic of the complete system, including the microwave source and detector, and is not an intrinsic property of the broadband cell.

Sensitivity Compared to Conventional EPR Spectrometers. To get an impression of the sensitivity of the instrument in comparison with conventional single-frequency spectrometers I measured the signal of a small-volume wire microstrip reflection cell (4 μL) filled with dpph at dip frequencies close to those of our S-band and X-band spectrometers and then used an equivalent sample in our

DOI: 10.1021/acs.jpca.9b03574
J. Phys. Chem. A 2019, 123, 6986−6995

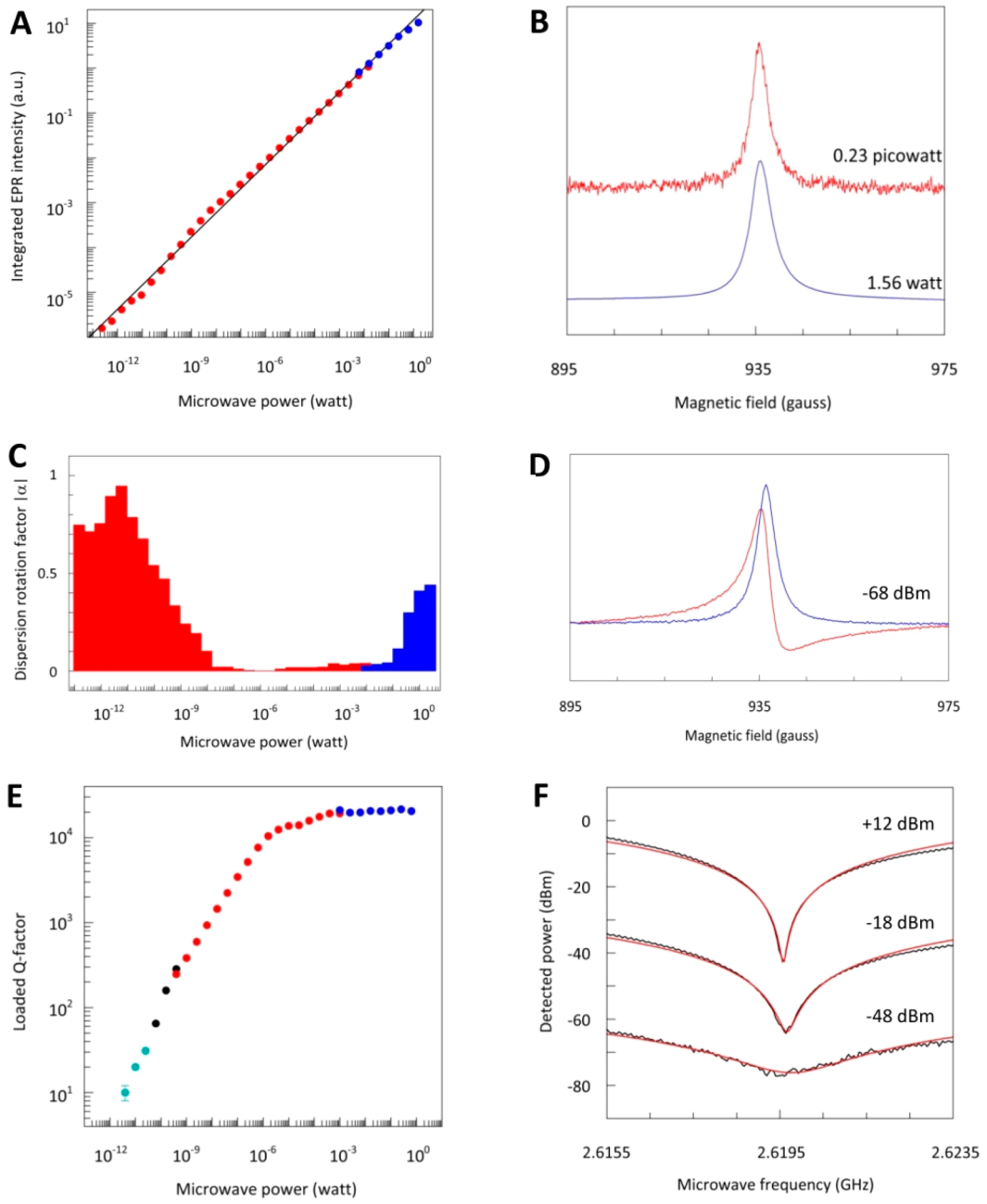

Figure 4. Power-response tests of the wire micro strip cell. (A) Integrated absorption intensity of solid dpph is linear in the incident microwave power over 13 decades. (B) Spectra at lowest and highest power employed. (C) Hilbert transformation to remove dispersion, as a function of incident power. (D) Example of spectrum before (red) and after (blue) dispersion correction. (E) Loaded Q factor of resonator-circuit dip near 2.62 GHz versus incident power. Color code (from high to low power): blue, data obtained with 43 dB amplifier; red, no amplifier used; black, span to determine dip Q factor extended from 8 to 45 MHz; cyan, span extended to 70 MHz. (F) Examples of resonator dip pattern for different incident powers.

split-ring S-band cavity and our standard rectangular X-band cavity to measure the signal either by direct detection (i.e., cavity connected to the VST via an appropriate circulator but with mode tuning using the cavity iris in the absence of a tuning phase shifter) or by conventional 100 kHz field-modulation spectroscopy using a modulation amplitude of 0.5 G. In all six cases the noise level was monitored at constant, off-resonance magnetic field for the same scan time as used for the signal detection. Root-mean-square noise amplitude was determined by numerical analysis using the Basic RMS subroutine available in LabVIEW's Waveform Measurements palette. Signal intensity was measured as peak-to-peak amplitude of the unfiltered first-derivative spectra. Resulting S/N levels are presented in Table 1.

Under the employed instrument settings direct detection with the VST using a regular cavity is only mildly less sensitive than conventional field-modulation detection with the same cavity. More remarkably, with the present state-of-the-art of the broadband wire micro strip reflection cell, the S/N levels obtained in this particular case are only an approximate factor of 5 below the levels of the single-frequency cavity-based experiments. Generalization of this condition would imply that,

DOI: 10.1021/acs.jpca.9b03574
J. Phys. Chem. A 2019, 123, 6986−6995

Table 1. Sensitivity Comparison for Constant Sample Size[a]

mode of detection	S-band freq (MHz)	S-band S/N	X-band freq (MHz)	X-band S/N
regular EPR with field modulation	4037	978	9871	1704
regular cavity with VST	4038	714	9871	1250
wire micro strip resonator with VST	3683	237	9829	321

[a]The signal of a dpph powder sample of 4 μL volume was measured under standardized conditions of 100 G scan range, −20 dBm microwave power, no RC-filtering, 120 s acquisition time, and (when applicable) 0.5 G modulation, with the indicated setups. All resulting 1024-point spectra were subjected to 6-point Savitzky−Golay filtering. Signal-to-noise (S/N) values are reported as ratios of the peak-to-peak amplitudes of the signal and the noise in the first-derivative spectrum.

where the recording of a good quality spectrum with an X-band spectrometer typically takes some 3 min, obtaining comparable quality data anywhere in the 0.5−12 GHz frequency range with the present setup would require some $3 \times 5^2 = 75$ min.

Broadband EPR of Low-Symmetry Cu(II) Complex. A preparation of 0.5% Cu(II) in diamagnetic $ZnSO_4 \cdot 1H_2O$ finely ground powder was taken as a realistic spectroscopic test system. The $ZnSO_4 \cdot 1H_2O$ crystal is monoclinic[9] and $CuSO_4 \cdot 1H_2O$ is triclinic.[10] The all-oxygen ligation excludes a superhyperfine interaction, and the 1:200 Cu:Zn dilution minimizes dipolar interaction between copper centers. Furthermore, since the sample is a dry powder, the strong variation of line width with nuclear quantum number m_I and with microwave frequency that is typically observed in frozen aqueous solutions of copper complexes as a consequence of strain,[11] was anticipated to be absent or at least inextensive. Thus, the spin Hamiltonian for this low-symmetry $3d^9$ system with $S = 1/2$, $I = 3/2$ is one of considerable, but perhaps not overwhelming complexity:

$$H = \beta \mathbf{B} \cdot \bar{\bar{\mathbf{g}}} \cdot \mathbf{S} + \mathbf{S}(\mathbf{R}^{-1}\bar{\bar{\mathbf{A}}}\mathbf{R})\mathbf{I} + \mathbf{I}(\mathbf{R}_2{}^{-1}\bar{\bar{\mathbf{P}}}\mathbf{R}_2)\mathbf{I} \quad (8)$$

in which **g**, **A**, and **P** are diagonal, rhombic matrices/tensors, **R** is the Euler rotation matrix that relates the Cartesian axis system that diagonalizes the hyperfine matrix **A** with that in which **g** is diagonal, and $\mathbf{R}_2$ is the rotation matrix that diagonalizes the quadrupole tensor **P** (Supporting Information, part F, Hamiltonian).

Low-temperature data were collected at multiple frequencies from 0.8 to 11 GHz. Data taken with conventional spectrometers at the X- and Q-bands were added as benchmarks of sensitivity and resolution. Figure 5 is an overview of the resulting spectra plotted on a reciprocal **g** value scale (or linear energy scale) as the abscissa and the microwave frequency as the ordinate for the spectral baselines, which is one out of several possible 2D presentations, this one emphasizing the nonlinear reduction of the hyperfine structure with increasing frequency. The complete set exhibits an unprecedented richness of fine spectral details: at higher frequencies a hyperfine splitting of considerable magnitude along g_x is clearly resolved. The g_z four-line hyperfine pattern at higher frequencies is straightforward with equidistant peaks of equal width except for a slight broadening at the extremes due to the presence of the two natural abundant isotopes ^{63}Cu (~69%) and ^{65}Cu (~31%).

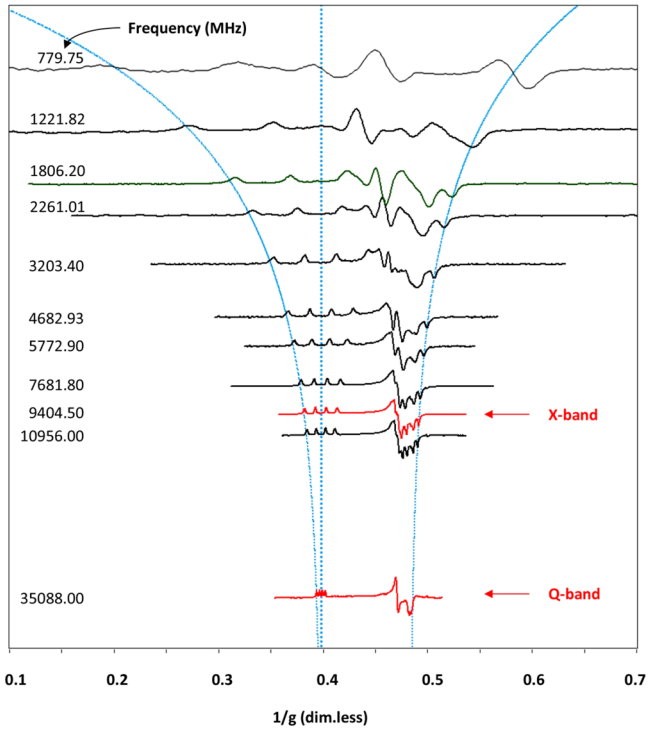

Figure 5. Field-frequency 2D plot of 0.5% Cu(II) in $ZnSO_4$ from 0.8 to 35.1 GHz. The signal was measured at the nine indicated frequencies, and the set was augmented with data obtained with regular X-band and Q-band spectrometers. For the broadband machine a wire micro strip resonator was used with a sample volume of 70 × 27 × 0.2 mm on both sides, i.e., a total volume of 0.75 mL. Spectra were collected by averaging over 30−80 min at an incident power level 1 mW and a sample temperature of 16 K. The X-band spectrum was taken in 4 min with 0.2 mW, 2 G modulation, and 16 K. The Q-band spectrum was collected in 12 min with 20 mW, 10 G modulation, and 34 K. The magnetic-field scale of all spectra has been replotted on a reciprocal **g** value scale, $1/\mathbf{g} = \beta\mathbf{B}/h\nu$. Vertical broken blue lines correspond to the first hyperfine line with $\mathbf{B} = \mathbf{B}(g_z) - 1.5A_z$, the g_z value (straight line), and the last hyperfine line with $\mathbf{B} = \mathbf{B}(g_x) + 1.5A_x$.

As an illustration of how we can go about analyzing such a data set Figure 6 shows simulations at high (Q-band: 35.088 GHz), intermediate (C-band: 5.772 MHz), and low (L-band: 1.221 GHz) frequency. In the left-hand panels the Cu(II) electronic structure is modeled as being of orthorhombic symmetry, in the right-hand panels triclinic symmetry is assumed congruent with crystal structure.[9,10] Spectroscopically, the key difference between the two sets is that in the lower symmetry the **g**- and **A**-matrices in the spin Hamiltonian are not diagonal in the same axes system. Attempts to explore the occurrence of lower than orthorhombic symmetry in the EPR of randomly oriented coordination complexes are rare.[12,13] In spectral analysis by simulation it is common to probe only isotropic, axial, and rhombic powder patterns. The customary approach is that of using an analytical expression deduced with perturbation theory in which the metal hyperfine interaction is taken as a perturbation, up to second order, of the electronic Zeeman interaction. For orthorhombic symmetry the relevant expression was deduced for frequency-swept spectra by Pake and Estle in 1971 (eqs B15−B17 in ref 14), and I have rewritten their result for the more practical situation of field-swept spectra (eqs 5.18−5.33 in ref 15). Analytical perturbation expressions for power patterns of lower than

DOI: 10.1021/acs.jpca.9b03574
J. Phys. Chem. A 2019, 123, 6986−6995

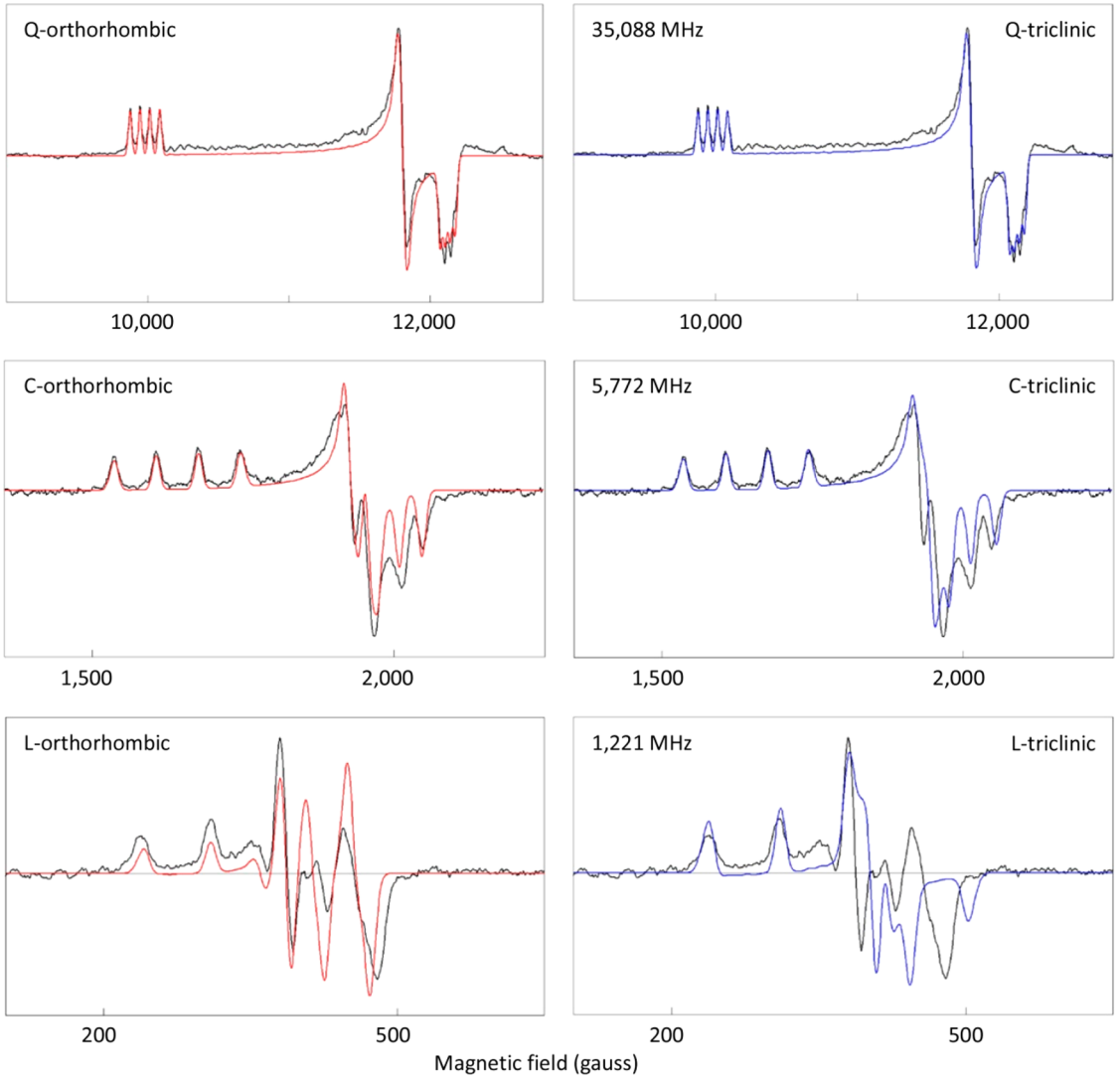

Figure 6. Orthorohombic and triclinic symmetry based simulations of the Cu site in Q-, C-, and L-bands. The experimental data are from Figure 5. All simulations are based on a single set of **g** values: g_{zyx} = 2.5115, 2.1235, 2.0675. The orthorhombic **A** values (gauss) are A_{zyx} = 69, 9, 35; the triclinic values are A_{zyx} = 75, 0, 0 with rotation (degrees) α = +24 and β = +20. The numbers apply to ^{63}Cu; the simulations are for natural abundance ^{63}Cu + ^{65}Cu. In all cases quadrupolar interaction is not resolved; i.e., the **P** matrix is zero. Gaussian line widths (standard deviation in gauss) are isotropic 5 in the L-band and 6 in the C-band, and W_{zyx} = 12, 23, 14 (orthorhombic) or 13, 22, 14 (triclinic) in the Q-band. The orthorhombic symmetry based simulation is consistent over the full frequency range (ignoring a variation in line width with nuclear orientation), and the triclinic symmetry based simulation is not.

orthorhombic symmetry have not been published. For the present situation the perturbation approach will not suffice because the assumption that a copper hyperfine interaction is a perturbation to a copper Zeeman interaction breaks down at, and below, L-band frequencies.[15] I therefore used a simulator based on full-blown energy matrix diagonalization for position and intensity computation which is valid for any ratio of hyperfine over Zeeman interaction. This approach has the added advantage that extension to more complex Hamiltonians, in particular to triclinic symmetry, and also to inclusion of copper quadrupolar interaction does not significantly increase the required computational time per simulation, and this makes a rigorous test on metal-site symmetry practical. Figure 6 is the result of such a test.

It is found that the high-frequency, Q-band data are equally well fit with either an orthorhombic Hamiltonian or a triclinic one. However, the underlying models are very different: orthorhombic symmetry requires the assumption of a rather unusually anisotropic **A**-matrix, while a triclinic-symmetry fit of equal quality is obtained assuming an axial **A**-matrix with dominant A_z term and small splittings (0−10 G) in the perpendicular direction (a pattern that abounds in the copper EPR literature over the last half a century) but here with rotation required between **g** and **A**. On the basis of this analysis of single-frequency data, one would be tempted to conclude that an appealing congruence exists indeed between electronic structure (triclinic) and crystal structure (triclinic). The multifrequency data now afford a rigorous test between the two models. Upon a 6-fold reduction in frequency to the C-band (the middle panels of Figure 6) the triclinic simulation, based on the parameters established in the Q-band, exhibits significant misfit in the *xy* region, while the orthorhombic simulation rather faithfully reproduces the C-band spectrum. With another 5-fold reduction in frequency to the L-band, the difference in quality of the two fits is even more pronounced. We are thus forced to revisit our conclusion that was based on

DOI: 10.1021/acs.jpca.9b03574
J. Phys. Chem. A 2019, 123, 6986−6995

the Q-band data alone: fits of the multifrequency low-temperature EPR data are consistent with orthorhombic symmetry and not with the room-temperature crystallographic triclinic symmetry.

As an aside, the fittings in Figure 6 led to some additional conclusions: introduction of finite quadrupolar terms in the Hamiltonian, be the **Q**-tensor collinear with **g**, or with **A**, or subject to a general rotation, never led to a quality increase, of any significance, of the fits. Apparently, copper quadrupolar interaction is not resolved in this multifrequency data set. Also, with this powder sample a variation of line width, W, with nuclear orientation, i.e., as a function of quantum number m_I, is in fact observed (contrast to initial expectation) in all frequency bands especially in the x direction. Such a pattern has been included in the past in copper simulations in the form of ad hoc expressions of the form $W = f(m_I)$, for example, $W = A + Bm_I + Cm_I^2$, but since its interpretation has until now not moved beyond a qualitative assignment to "strains".[15] I have not pursued this subject here. Also, the experimental data exhibit minor details that are not reproduced in the fits. This is particularly clear in the spectra in the 5−11 GHz range (Figure 5) where in the A_x pattern we consistently observe line asymmetries and also variation in the three splitting between the four hyperfine lines. A possible source for these small effects might be dipolar interaction between different copper sites of the 0.5% Cu-doped $ZnSO_4$ microcrystals. Inclusion of these effects in the energy-matrix diagonalization routine would be theoretically trivial but practically quite taxing: even inclusion of pairwise Cu−Cu interaction (dimer formation) only would increase the size of the energy matrix from 8 × 8 to 64 × 64. That dimerization indeed occurs is evident from X-band data taken at ambient temperature showing a half-field transition plus a broad spectrum underlying the monomeric copper spectrum (Supporting Information, part G, Dimerization). Finally, as a control experiment on the methodology, it was ascertained that, for the C- and Q-band spectra orthorhombic simulations based on the perturbation-theory expression gave fits identical to those from energy-matrix diagonalization.

DISCUSSION

The resonant cavity has been at the heart of EPR spectrometers from early on in the history of the spectroscopy. The first explicit reference to a microwave cavity, of undefined dimensions, for S-band EPR was in 1946 by Cummerow and Halliday.[2] Possibly even earlier, the discoverer of EPR spectroscopy, E. K. Zavoisky, may have used what appears to be a split-ring cavity also for the S-band.[16] Shortly thereafter, Bagguley and Griffiths reported an EPR study in which use was made of an X-band cavity, again of unspecified dimensions and geometry.[1] Since then, the single-mode (i.e., always operating at its fundamental frequency) either rectangular or cylindrical X-band cavity (9−10 GHz) became the de facto standard, which it still is today, as the result of a combination of practical determinants, in particular: relative ease of construction, availability of X-band sources, and favorable noise characteristics of detection diodes. Later, in response to the need of routinely collecting data at least at one other frequency for, e.g., systems with convoluted hyperfine and Zeeman interactions, a commercial Q-band (ca. 35 GHz) spectrometer was produced and was quickly adopted for studies of, for example, Cu(II)[17] or Mo(V)[18] proteins. In more recent times commercial continuous-wave (cw) spectrometers have become available from the L-band (ca. 1 GHz) to the J-band (ca. 263 GHz), and outside this range machines have been laboratory-built for subgigahertz[19] to terahertz[20] frequencies. In spite of these developments, multifrequency EPR has not become a routine practice in the study of transition ion complexes, presumably due to the excessive cost of investment and operational complexity. Furthermore, X-band flanking studies in the approximate 1−20 GHz range are relatively rare, which is remarkable in view of the fact that pronounced spectral changes with frequency are to be expected here, in particular for the many systems with significant central hyperfine interaction or with multicenter dipolar interactions such as powders of synthetic coordination compounds as well as complex metalloproteins. These problems are also not well addressed using the many special forms of advanced EPR based on double resonance and/or pulse techniques, which find their main field of application in the resolution of small superhyperfine interactions from ligands. A paradigm-changing approach would appear to be desirable: broadly frequency tunable measurements with a single spectrometer of sufficient sensitivity for the collection of high-quality cw EPR spectra from dilute, randomly oriented transition ion complexes.

This quest for a fundamental change has two key technical aspects: a broadly tunable source and direct-detection system and a broadly tunable resonator. For the frequency range of interest, e.g., 1−20 GHz, only a small number of relevant papers have appeared in the last half a century of EPR literature. In an early study (1962) use of a nonresonant, frequency-independent helix was proposed as a microwave delay line.[21] With a sample placed inside the helix, this structure is similar to the probe described here, but with the ground plate absent. A microcoil version with inner diameter of ca. 0.1 mm was later used to build a frequency-scanning (0.1−8.5 GHz) spectrometer with constant field, which was applied to strong samples of dpph and AgMn spin glass.[22] In a different vein, a broadly tunable (0.34−4.0 GHz) "cavity" was proposed with the helix surrounded by a ground plate in the form of a rectangular box.[23] No practical EPR applications were described. An early (1966) study on mechanically adjustable cavities in the 1.0−4.6 GHz range found no follow up, possibly because of limited stability of the tunable source, a modulated traveling wave tube.[24] A more recent attempt describes a similar resonator now for 4−40 GHz combined with a vector network analyzer with direct detection, but the sensitivity of the setup is not clear, as only single crystal samples of pure molecular magnets were measured.[25] An early (1974) attempt to use strip line as the basis for a broadband resonator was tested, using conventional S-band and X-band equipment, and was found to give reasonably good-quality spectra of Mn(II) contamination in MgO,[26] but again no follow up was reported. Several more recent papers describe the testing of sample cells based on either meandering micro strips[27,28] or coplanar thin films[29,30] with direct detection with a VNA, but more often with less sensitive diode-based power meters. Resolution appears to be oftentimes problematic, e.g., when a dpph line is found with a severely broadened fwhh line width of ca. 22 G[27] or when a nitronyl-nitroxide radical is found to give a single line[29,30] where regular EPR of these compounds is typically rich in hyperfine structure.[31] Also, detection of 0.2 μg of dpph with a signal-to-noise ratio of 121 may suggest an impressive absolute sensitivity,[28] but realizing that the sample is the dried out result of a 5 mM stock solution makes one aware that the concentration sensitivity is in fact

DOI: 10.1021/acs.jpca.9b03574
J. Phys. Chem. A 2019, 123, 6986−6995

rather poor; in chemical and biochemical applications of dilute transition ion EPR the *concentration* sensitivity is of far greater importance than the *absolute* sensitivity. Other studies have reported the use of analog or digital, scalar or vector network analyzers as source/detector of EPR[32−35] including my own work.[3] None of the cited papers provide examples of multifrequency data of high quality from randomly oriented, dilute transition ion complexes.

To my knowledge Figure 5 of the present paper is the first instance of such a milestone. It makes a mark of technical feasibility: the required equipment is not more complex and not more expensive than a standard commercial single-frequency spectrometer; in particular, the resonator is much simpler and cheaper than a standard cavity. It is also a mark of technical potential: concentration sensitivity is less than an order of magnitude below the present optimum of standard X-band equipment, and improvements can be envisioned (e.g., modulation of field or frequency). First and foremost, however, it outlines a new chemical goal for EPR spectroscopy of randomly oriented systems: a methodology for the reliable determination of molecular electronic structure based on analysis of field-frequency 2D data sets.

■ ASSOCIATED CONTENT

Supporting Information

The Supporting Information is available free of charge on the ACS Publications website at DOI: 10.1021/acs.jpca.9b03574.

A, cell design (isometric drawing and specific examples); B, theory (theoretical background of wire micro strip cell); C, mode patterns (resonance peak patterns in transmission and reflection cells); D, hardware (description of all spectrometer components); E, software (description of all programs for broadband spectrometer operation); F, Hamiltonian (numerical analysis of triclinic Cu(II) spin Hamiltonian); G, dimerization (formation of Cu−Cu pairs) (PDF)

BB_Program_Suite: a zip file containing all source files of the software developed for, and used in this study (ZIP)

■ AUTHOR INFORMATION

Corresponding Author

*E-mail: w.r.hagen@tudelft.nl.

ORCID

Wilfred R. Hagen: 0000-0002-1609-6671

Notes

The author declares no competing financial interest.

■ ACKNOWLEDGMENTS

This work was financially supported by the Department of Biotechnology, Delft University of Technology.

■ REFERENCES

(1) Bagguley, D. M. S.; Griffiths, J. H. E. Paramagnetic resonance and magnetic energy levels in chrome alum. *Nature* **1947**, *160*, 532−533.

(2) Cummerow, R. L.; Halliday, D. Paramagnetic losses in two manganese salts. *Phys. Rev.* **1946**, *70*, 433.

(3) Hagen, W. R. Broadband transmission EPR spectroscopy. *PLoS One* **2013**, *8*, No. e0059874.

(4) Hammerstad, E. O. Equations for microstrip circuit design. *5th European microwave conference IEEE Proceedings* **1975**, 268−272.

(5) Wheeler, H. A. Transmission-line properties of a strip on a dielectric sheet on a plane. *IEEE Trans. Microwave Theory Tech.* **1977**, *25*, 631−647.

(6) Wadell, B. C. *Transmission line design handbook*; Artech House; Norwood, MA, 1991; pp 113−114.

(7) IPC-2141A. *Design guide for high-speed controlled impedance circuit boards*; IPC: Northbrook, Ill, USA, 2004. See also: IPC-2141A Errata information.

(8) Ernst, R. R. Numerical Hilbert transform and automatic phase correction in magnetic resonance spectroscopy. *J. Magn. Reson.* **1969**, *1*, 7−26.

(9) Le Fur, Y.; Coing-Boyat, J.; Bassi, G. Structure des sulfates, monohydrates, monocliniques, des métaux de transition, MSO_4, H_2O (M = Mn, Fe, Co, Ni et Zn). *Compt. Rend. Acad. Sci. Paris* **1966**, *262*, 632−636.

(10) Giester, G. The crystal structures of $CuSO_4 \cdot H_2O$ and $CuSeO_4 \cdot H_2O$, and their relationships to kieserite. *Mineral. Petrol.* **1988**, *38*, 277−284.

(11) Froncisz, W.; Hyde, J. S. Broadening by strains of lines in the g-parallel region of Cu^{2+} EPR spectra. *J. Chem. Phys.* **1980**, *73*, 3123−3131.

(12) Pilbrow, J. R.; Winfield, M. E. Computer simulation of low symmetry E.S.R. spectra due to vitamin B_{12r} and model systems. *Mol. Phys.* **1973**, *25*, 1073−1092.

(13) Greenwood, R. J.; Wilson, G. L.; Pilbrow, J. R.; Wedd, A. G. Molybdenum(V) sites in xanthine oxidase and relevant analog complexes: comparison of oxygen-17 hyperfine coupling. *J. Am. Chem. Soc.* **1993**, *115*, 5385−5392.

(14) Pake, G. E.; Estle, T. L. *The physical principles of electron paramagnetic resonance*, second ed.; W.A. Benjamin Inc.: Reading, MA, 1971.

(15) Hagen, W. R. *Biomolecular EPR spectroscopy*; CRC Press, Taylor & Francis Group, Boca Raton, FL, 2009.

(16) Schweiger, A.; Jeschke, G. *Principles of pulse electron paramagnetic resonance*; Oxford University Press, 2001.

(17) Aasa, R.; Aisen, P. An electron paramagnetic resonance study of the iron and copper complexes of transferrin. *J. Biol. Chem.* **1968**, *243*, 2399−2404.

(18) Bray, R. C.; Vänngård, T. 'Rapidly appearing' molybdenum electron-paramagnetic-resonance signals from reduced xanthine oxidase. *Biochem. J.* **1969**, *114*, 725−734.

(19) Eaton, G. E.; Eaton, S. EPR spectrometers at frequencies below X-band. In *EPR: instrumental methods*; Berliner, L. J., Bender, C. J., Eds.; Kluwer Academic/Plenum Publishers: New York, NY, 2004.

(20) Lu, J.; Ozel, I. O.; Belvin, C. A.; Li, X.; Skorupskii, G.; Sun, L.; Ofori-Okai, B. K.; Dincă, M.; Gedik, N.; Nelson, K. A. Rapid and precise determination of zero-field splittings by terahertz time-domain electron paramagnetic resonance spectroscopy. *Chem. Sci.* **2017**, *8*, 7312−7323.

(21) Webb, R. H. Use of traveling wave helices in ESR and double resonance spectrometers. *Rev. Sci. Instrum.* **1962**, *33*, 732−737.

(22) Mahdjour, H.; Clark, W. G.; Baberschke, K. High-sensitivity broadband microwave spectroscopy with small nonresonant coils. *Rev. Sci. Instrum.* **1986**, *57*, 1100−1106.

(23) Frénois, C. Broadband tunable cavities with helical microstrip lines. *J. Phys. E: Sci. Instrum.* **1984**, *17*, 35−39.

(24) Erickson, L. E. Electron-paramagnetic-resonance absorption by trivalent neodymium ions in single crystals of lanthanum trichloride and lanthanum ethyl sulphate in zero magnetic field. *Phys. Rev.* **1966**, *143*, 295−303.

(25) Schlegel, C.; Dressel, M.; van Slageren, J. Broadband electron spin resonance at 4−40 GHz and magnetic fields up to 10 T. *Rev. Sci. Instrum.* **2010**, *81*, No. 093901.

(26) Johansson, B.; Haraldson, S.; Pettersson, L.; Beckman, O. A stripline resonator for ESR. *Rev. Sci. Instrum.* **1974**, *45*, 1445−1447.

(27) Tsai, C. C.; Choi, J.; Cho, S.; Lee, S. J.; Sarma, B. K.; Thompson, C.; Chernyashevskyy, O.; Nevirkovets, I.; Ketterson, J. B. Microwave absorption measurements using a broad-band meanderline approach. *Rev. Sci. Instrum.* **2009**, *80*, No. 023904.

DOI: 10.1021/acs.jpca.9b03574
J. Phys. Chem. A 2019, 123, 6986−6995

(28) Chen, Z.; Sun, J.; Wang, P. Broadband ESR spectroscopy with a tunable interferometer. *IEEE Trans. Magn.* **2017**, *53*, 4001909.
(29) Clauss, C.; Bothner, D.; Koelle, D.; Kleiner, R.; Bogani, L.; Scheffler, M.; Dressel, M. Broadband electron spin resonance from 500 MHz to 40 GHz using superconducting coplanar waveguides. *Appl. Phys. Lett.* **2013**, *102*, 162601.
(30) Wiemann, Y.; Simmendinger, J.; Clauss, C.; Bogani, L.; Bothner, D.; Koelle, D.; Kleiner, R.; Dressel, M.; Scheffler, M. Observing electron spin resonance between 0.1 and 67 GHz at temperatures between 50 mK and 300 K using broadband metallic coplanar waveguides. *Appl. Phys. Lett.* **2015**, *106*, 193505.
(31) Ullman, E. F.; Osiecki, J. H.; Boocock, D. G. B.; Darcy, R. Studies of stable free radicals. X. Nitronyl nitroxide monoradicals and biradicals as possible small molecule spin labels. *J. Am. Chem. Soc.* **1972**, *94*, 7049−7059.
(32) Görlitz, D.; Kapoor, J.; Kötzler, J. Vector network analysis in swept-frequency microwave spectroscopy at low temperatures. *J. Phys. E: Sci. Instrum.* **1989**, *22*, 884−885.
(33) Rubinson, K. A. Broadband (up to 10 GHz) electron-paramagnetic-resonance spectrometer: cw implementation with direct detection. *Rev. Sci. Instrum.* **1989**, *60*, 392−395.
(34) Jang, Z. H.; Suh, B. J.; Corti, M.; Cattaneo, L.; Hajny, D.; Borsa, F.; Luban, M. Broadband electron spin resonance at low frequency without cavity. *Rev. Sci. Instrum.* **2008**, *79*, No. 046101.
(35) Tseitlin, M.; Quine, R. W.; Rinard, G. A.; Eaton, S. S.; Eaton, G. R. Digital EPR with an arbitrary waveform generator and direct detection at the carrier frequency. *J. Magn. Reson.* **2011**, *213*, 119−125.

DOI: 10.1021/acs.jpca.9b03574
J. Phys. Chem. A 2019, 123, 6986−6995